A Guideline for Modeling Voltage and Frequency Controls in AC Microgrids: The Influence of Line Impedance on Transient Time

M. Majidi, F.M. Ibanez, D. Pozo
Center for Energy Science and Technology
Skolkovo Institute of Science and Technology
Mosow, Russia
(maryam.majidi, fm.ibanez, d.pozo)@skoltech.ru

A.A. Nazeri
Department of Electrical Engineering and
Computer Science, University of Kassel
Kassel, Germany
ahmadali.nazeri@skoltech.ru

***Abstract*—Microgrids (MG) were first conceived as small-scale grids working in an islanding-mode. However, they can be operated in a grid-connected mode too. MGs can easily host a large number of paralleled-connected distributed generations (DGs). The increased penetration of the renewable energy sources (RESs) is raising new concerns about redesigning the role of MGs for supporting and regulation services of power grids at the system level. The operation of MGs could provide support for voltage and frequency regulation while ensuring uniform power flow in both directions. In this regard, MGs can relieve the stress of the main transmission system, decrease feeder losses, and increase system power quality. In order to inject current, a proper design of the control system parameters of the AC MGs is needed to ensure the exact parameters of the amplitude and synchronized frequency. In this paper, we present a step-by-step methodology for designing control systems for MGs. The primary and secondary control loops of the voltage and frequency of the three-phase paralleled connected voltage source inverter-based (VSI) MG are derived. In addition, we study the impact of DGs remoteness. The primary and secondary control loops are based on the droop control and autonomous frequency control system. The control systems are modeled and simulated in MATLAB/Simulink.**

***Index Terms*—Droop control, frequency controller, micro grid, voltage controller, voltage source inverter.**

I. Introduction

Over the last decade, power systems have experienced a large integration of the RESs, as DGs that are mainly connected at low voltage (LV) and medium voltage (MV). Power electronics play a key role in tackling challenges aroused from RESs in terms of control with reduced or almost zero inertia. For instance, grid-connected converters have been widely used in AC MGs [1]. The integration of the parallel DGs with loads in medium and low voltage distribution systems is presented in [2]. The interfacing between MGs and devices such as RESs, distributed energy storage systems and active loads are good examples of the importance of power electronic converters for addressing the control in inertial-less systems. MGs can operate in two different modes: grid-connected mode and islanded-mode. In grid-connected mode, LV MGs are connected to the main MV network. When the main grid is disconnected, the MG operates as an islanded-mode of operation where the MG delivers the power to the local/critical connected load. Autonomous MGs are weaker than conventional power systems due to the lower inertia [3]. Islanded MGs are appropriated for the electrification of autonomous and remote systems such as in rural areas [4].

Regarding AC MGs, parallel connected VSIs are commonly used as a power electronics interface [5]. However, the integration of the RES to the MGs leads to many issues such as power imbalance, frequency fluctuations, harmonic distortion and reduction in the overall efficiency of the system.

During the last years, various MG control techniques have been investigated. For instance, [6], [7], [8] addressed different aspects of the AC MGs comparing various frequency and voltage control techniques for inverter-based MGs. In [9], the authors presents a control design and stability analysis of the parallel connected three-phase VSIs. A MG of uninterruptible power supply systems connected in parallel is presented in [10], applying a droop control strategy, thus not including any central controller. A multivariable-droop synchronous current converter control strategy where the synchronization and load management works together in a single controller to control the current of MGs is studied in [11]. An advanced energy management structure, which is aimed to coordinately manage the demand response and distributed generation resources by constructing a hierarchical frequency control structure is introduced in [12].

Designing a proper control algorithm is crucial to provide efficient operation and stability of the MGs. Frequency and voltage regulation, active and reactive power control between DGs and the main grid, synchronization of MGs with the network and energy management are the goals that can be achieved by applying an appropriated control structure. The primary control is a decentralized and an independent control

This work was supported by Skoltech NGP Program (Skoltech-MIT joint project).

structure, which can be implemented by the voltage and current control loops, droop controller with virtual impedance. In the secondary control, MGs' central control, such as frequency synchronization, frequency and voltage restoration, reactive power compensation are considered to achieve comprehensive control of MGs [13], [14], [15].

Extensive research has been carried on the distributed control systems. However, there has been little attention to the methodology for selecting proper control parameters of the MGs. This paper provides a modest and comprehensive design guideline of a three-phase VSI based AC MGs, which considers that the inverter is fully self-governing; this means that the inverter synchronizes with the grid and shares the power consumption with the other sources. For validating the design procedure, MATLAB/Simulink simulation results of a small MG, which consists of two VSIs connected in parallel at the point of common coupling (PCC) at different distances are presented. In addition, the time response of the system is measured for different design parameters and the stability margins are derived.

This paper is structured as follows. In Section II, the system modeling and the design of the controllers for the system is presented. Section III presents the guidelines of the droop based primary control for the system. Section IV reviews the secondary control structure for voltage amplitude and frequency recovery. Section V presents the simulation results of the paralleled three-phase VSIs. Finally, conclusion is given in Section VI.

II. System Modeling

The schematic block diagram of the proposed control system of the AC MG is shown in Fig. 1. The proposed control is divided into the primary and secondary control. Besides, the power processing sector of the AC MG contains a three-leg inverters, a space vector pulse width modulation (SVPWM) and an output *RL* filter.

The following equations state the minimum total load impedance and the filter inductance as a function of the inverter output power and voltage

$$R_l = \frac{{V_o}^2}{S_n} \tag{1a}$$

$$R_l \cdot \frac{V_b - V_o}{V_o \cdot \omega_0} \leq L_s \leq R_l \cdot \frac{3\left(V_b\sqrt{3}\right)^2}{10S_n \cdot \omega_0}. \tag{1b}$$

where R_l is the minimum load impedance (Ω), S_n is the nominal apparent power of the inverter (VA), V_b is the line voltage (V), the V_o is the minimum output voltage that is considered as 90% of the V_b (V), ω_0 is the nominal frequency of the system (rad/s) and L_s is the filter inductance (H).

In the proposed control system, the primary controller includes active and reactive power controller, droop and voltage controller and Parks-to-Clark transformation blocks; where the three phase voltages as V_{abc} are transformed to the synchronous rotating reference frame as V_{dq0} by Parks transformation. The second control level contains synchronization of the control loops and frequency controller to synchronize and control the frequency of the system.

III. Primary Control

Conventionally, the P/ω and Q/E droop control are adopted as the decentralized control approaches in power electronics based MGs for the islanded-mode. Avoiding critical communication links among parallel-connected inverters is the main advantage of applying the droop control method [16]. The absence of communication links between parallel-connected inverters grants significant flexibility and high reliability [15]. In this study, the control structure is divided into two different parts. The first part is an external power calculation loop, which sets the magnitude and frequency for the primary control of the VSI output voltage along with droop characteristics set for the real and reactive powers. The second part is the voltage control loop to reject high-frequency disturbances and provide sufficient damping for the output *RL* filter.

However, the conventional droop control technique has several drawbacks such as slow transient response, inherent trade-off between voltage regulation and load sharing, poor harmonic, poor load sharing between the parallel-connected inverters in the case of the non-linear loads, line impedance mismatch, and poor performance with RESs [17], [18], [19]. In the proposed control system, exclusive of reconfiguration of the conventional droop system by dynamic estimation of parameters and utilizing the secondary control are some of these disadvantages, which are adjusted.

A. Power Calculation

The droop control method follows a similar functioning as the conventional power system, which reduces the reference frequency when there is a step change in the load to control the voltage and frequency. It is necessary to calculate the instantaneous active and reactive output powers to carry out the droop functions. The instantaneous values of the active and reactive powers can be calculated as

$$\tilde{p} = V_d I_d + V_q I_q \tag{2a}$$

$$\tilde{q} = V_d I_q - V_q I_d. \tag{2b}$$

The $\tilde{p}$ and $\tilde{q}$ are the instantaneous active and reactive powers, V_{dq0} and I_{dq0} are the output voltage and current in $dq-$frame. To get the active and reactive powers, the instantaneous power components are passed through a low-pass filter with a cut-off frequency lower than the bandwidth of the closed-loop of the system. It is given in (3a) and (3b).

$$P = \frac{\omega_c}{s + \omega_c} \cdot \tilde{p} \tag{3a}$$

$$Q = \frac{\omega_c}{s + \omega_c} \cdot \tilde{q} \tag{3b}$$

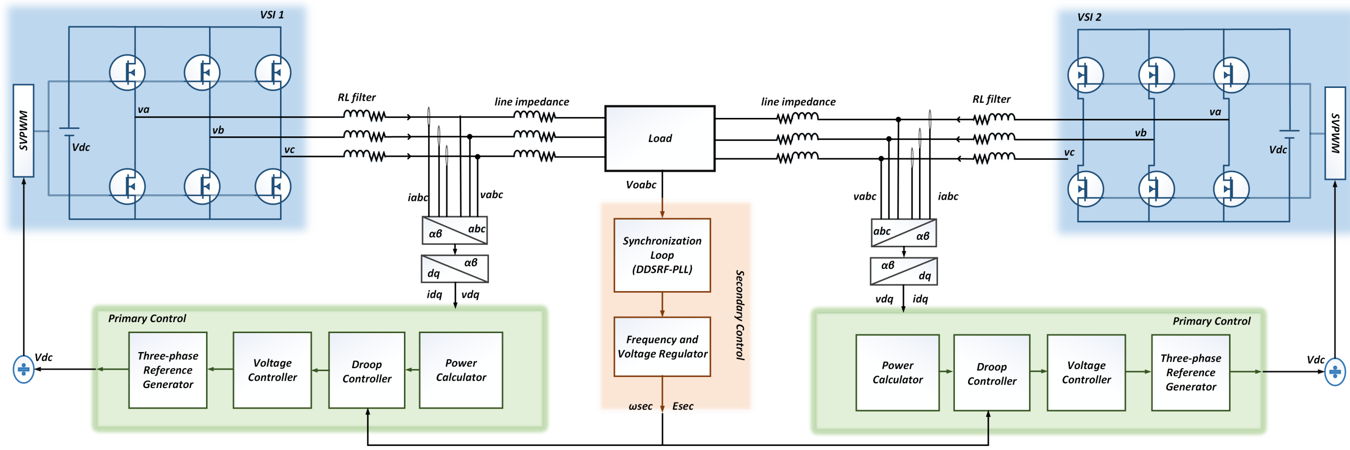

Figure 1. Block diagram of the control system of the three phase paralleled islanded AC MG VSIs.

where P and Q depicts real and reactive powers respectively and ω_c is the cut-off frequency of the low-pass filter, which should be less than the nominal frequency (ω_0) of the system.

B. Droop Control

The active and reactive powers of the MG with inductive impedance are defined as

$$P = \frac{EV}{X}\sin\varphi \tag{4a}$$

$$Q = \frac{EV\cos\varphi - V^2}{X}. \tag{4b}$$

where E is the voltage before the RL filter and V is the voltage at the output of the inverter. The small phase difference between E and V ($\sin\varphi \approx \varphi$ *and* $\cos\varphi \approx 1$), it is observed that P and Q mainly depends on φ and V. Consequently, P and Q can be controlled by means of the phase and amplitude of the output voltage respectively. The equations of the droop characteristics of P/ω and Q/E can be written as

$$\omega = \omega^* - m_p \cdot P \tag{5a}$$

$$E = E^* - n_q \cdot Q. \tag{5b}$$

where

$$m_p = \frac{\Delta\omega}{2P_{max}} \tag{6a}$$

$$n_q = \frac{\Delta E}{2Q_{max}}. \tag{6b}$$

The frequency (ω) is set according to the m_p and phase θ is set by the integration of the frequency. The ω^* and E^* being the nominal frequency and amplitude output voltage at no load where m_p and n_q are the frequency and amplitude droop coefficients respectively. Note that in conventional droop function m_p is equal to $\Delta\omega/P_{max}$, but in this case, as the inverter can absorb active power then m_p is calculated as in (6a). It is well known that if droop coefficients are increased, then good power sharing is achieved at the expense of degrading the voltage and frequency regulation. Moreover, $\Delta\omega$ and ΔE are the maximum allowed deviation of the frequency and voltage respectively. P_{max} and Q_{max} are the nominal active and reactive power supplied by the system respectively.

C. Primary Voltage Controller

The control strategy is chosen such that the output voltage magnitude reference is aligned to the d-axis of the inverter reference frame and the q-axis reference is set to zero. The algebraic equations of the voltage controller including all feedback and feedforward terms are formulated as

$$V_{d\_in} = V_{d\_o} - i_q\omega_0 L_s + K\left(1+\frac{1}{sT_i}\right)\left(V_{d-ref} - V_{d\_o}\right) \tag{7a}$$

$$V_{q\_in} = V_{q\_o} + i_d\omega_0 L_s + K\left(1+\frac{1}{sT_i}\right)\left(V_{q-ref} - V_{q\_o}\right). \tag{7b}$$

where V_{dqin} is the dq-frame of the SVPWM gate voltages, V_{dqo} is the measured ouput voltage. The K and T_i are the control parameters of the PI controller. The open loop transfer function of the voltage control loop is defined in (8), which includes the PI controller, the SVPWM time delay and the RL filter. By comparing the closed loop transfer function to the standard form, the values of K and T_i are defined.

$$G_{V\_ol}(s) = K\left(1+\frac{1}{sT_i}\right)\left(\frac{1}{1+sT_d}\right)\left(\frac{1/R_s}{1+sL_s/R_s}\right) \tag{8}$$

The K and T_i parameters of the voltage controller are derived by the pole placement method by comparing the closed loop voltage control with the standard form of the third order as

$$G_{V\_cl}(s) = \frac{{\omega_n}^3}{s^3 + s^2\omega_n(\alpha+2\zeta) + s{\omega_n}^2(1+2\zeta\alpha) + \alpha{\omega_n}^3}. \tag{9}$$

where the ω_n is the natural frequency of the system, which is calculated by the standard formula in (10) based on the system setting time and 0.01% criterion:

$$\omega_n = -\frac{\ln(0.01\%)}{\zeta T_s}. \tag{10}$$

where the settling time (T_s) is equal to $-\ln(0.01\%)\ 2.8T_d$ and ζ is the damping ratio, which is positive value in the range of $0 \leq \zeta \leq 1$. For the above system, T_d is the delay time caused by SVPWM, which is considered as the half of the switching time (T_s).

IV. Secondary Control

In the absence of communication links among VSIs, if one DG adjusts its droop controller, the other DGs would not discern this from a load step. Thus the droop shifting would potentially not be done equally by all DGs. Subsequently, this leads to unbalanced load sharing issues. The droop controller of each DG has to be tuned after every alteration of load or generation inside the MG. To regulate toward zero of any steady-state errors and restore and recompense frequency and voltage variation while sustaining load sharing. Execution of the secondary frequency control system, which can operate either in a decentralized or centralized modes of operation, solves the aforementioned problems.

In general, adjusting steady-state frequency deviations during any off-grid settings should be considered as one of the noteworthy objectives for any control approach. The secondary control contains a synchronization loop to extract the load/grid frequency and send the value to the secondary loop to adjust the frequency and eliminate the error. The secondary loop is the frequency and voltage regulator that send signals to the primary controller of each DG.

A. Frequency Detector

The decoupled double synchronous reference frame phase locked loop (DDSRF-PLL) is a three phase synchronous PLL based on the dq-frame, which is rotating with both positive and negative synchronous speeds respectively. The schematic block diagram of the DDSRF-PLL is shown in Fig. 2.

DDSRF allows the decoupling of the influence of negative sequence voltage component on the dq signals sensed by the SRF rotating with positive angular speed and vice versa, which makes the potential precise grid synchronization even under unbalanced grid faults. The decoupling network of this improved PLL completely suppresses the oscillations at the 2ω on the dq^{+1} and dq^{-1} reference frame signals. As a result, there is no need to decrease the bandwidth of

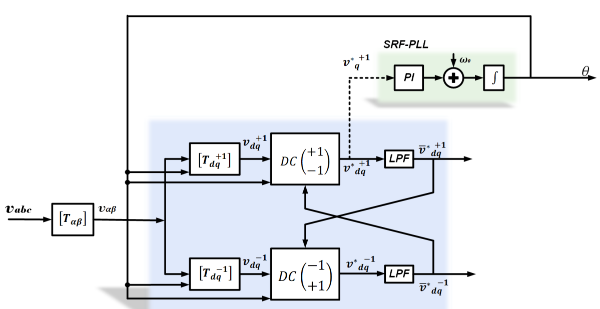

Figure 2. Schematic block diagram of the DDSRF-PLL

the PLL to reduce such oscillations and the real amplitude of the unbalanced input voltage sequence components are precisely detected [20]. The open-loop transfer function of the DDSRFPLL, which contains the loop filter (LF) and the voltage–controlled oscillator (VCO), is defined as

$$G_{PLL\_ol}(s) = K_{pll}\left(1 + \frac{1}{sT_{ipll}}\right)\left(\frac{1}{s}\right). \tag{11}$$

To calculate the PI parameters, the closed-loop transfer function is compared to the standard form of the second order system that is defined in (12).

$$G_{cl}(s) = \frac{s^2}{s^2 + s2\zeta\omega_n + \omega_n^2} \tag{12}$$

In this case, K_{pll} and T_{ipll} should be normalized, divided by the base voltage amplitude. Also, the natural frequency (ω_n) is defined from (10).

B. Frequency and Voltage Controller

The secondary voltage control open loop transfer function is given as

$$G_{vsc\_ol}(s) = K_{vsc}\left(1 + \frac{1}{T_{ivsc}s}\right)\left(\frac{1}{1 + sT_{dsc}}\right). \tag{13}$$

where T_{dsc} is the delay produced by the secondary control. To get positive value for the PI parameters, the closed loop transfer function is compared to (12) by considering setting time (T_{svsc}), constraint as less than $-\ln(0.01\%)\ 2T_{dsc}$.

The third order frequency transfer function is given:

$$G_{\omega sc\_ol}(s) = K_{fsc}\left(1 + \frac{1}{sT_{ifsc}}\right)\left(\frac{1}{1 + sT_{dsc}}\right)\left(\frac{1}{s}\right) \tag{14}$$

Similar procedure has been applied to design the PI controller comparing the closed loop transfer function with (9), by considering settling time ($T_{s\omega sc}$), greater than the $-\ln(0.01\%)\ 2T_{dsc}$.

V. Simulation Results

An AC MG is simulated in MATLAB/Simulink. The model consists of two paralleled VSI with RL filter, PI controller, voltage controller, active power sharing among DGs and frequency deviation are studied in this section. The system details are tabulated in Table I. In this study, as the R_l is the minimum load, the initial value of the resistive load is $3R_l$. When a step change in load is applied, the second load of $1.5R_l$ is connected and the total load becomes R_l. Likewise, the virtual impedance is a variable series impedance along the line impedance. Thus, it can be used to adjust the transient time of the power-sharing among the DGs. The control system parameters are shown in Table II. In this study, ζ is considered as 0.7071. In order to access the design of the system, it is essential to analyze the frequency response of each control loop.

Figure 3 shows the Bode diagram of the different control systems (primary voltage control, PLL and the secondary controls). The frequency bandwidth is around 50 Hz, as the frequency data is appropriate for the low bandwidth communication. Table III shows the stability margins of the suggested control systems. The gain margin indicates how much the controller gain can be increased before reaching the stability limit and the phase margin tells the amount of phase lag needed to reach the stability limit. Moving forward to the infinite gain margin means that the system will never become unstable, however increasing the gain adds more noise and transiency.

Fig. 4a shows the three phase sinusoidal output voltage waveform of the islanded-mode AC MG when supplying power to the load. Notice that, at $t_1 = 0.05$ s, the second inverter is synchronized to the first one in parallel operation and at $t_2 = 0.2$s, a step-change in the resistive load is applied. Fig. 4b shows the transient time of the voltage amplitude to reach to the nominal peak value for different distances of the paralleled DGs. Note that when the distance is less than 4 km, the system reaches the peak voltage in less than 20 ms. However, the transient time increases for longer distances.

Fig. 5 shows the two paralleled VSIs sharing the load using the droop method and the direct effect of distance on the transient time. The effect of equal distances on the transient time is less than the effect of the unequal distances. For example, for a distance of [5,5] km the transient time is 30.27 ms where the total line distance is 10 km, but for the distance of [5,3] km, the time is 173.95 ms. However, the transient time to reach the steady state point of each case study is different because of the varying line impedance. That is, after injecting the second DG and changing load, both inverters are able to sense the changes immediately and share the power at the same time due to applying the secondary control system.

Frequency error from nominal frequency is shown in Fig. 6. It shows that the grid frequency gets minor deviations due to

TABLE I. Power Stage Information

Parameter		Value	Description
f_0	[Hz]	50	System frequency
T_d	[s]	5.0000e-05	SWPWM time delay
f_s	[Hz]	10000	SWPWM switching frequency
V_{base}	[V]	338.8461	Line to neutral voltage (peak)
V_{dc}	[V]	677.6922	DC voltage source
P_{max}	[kW]	15	Nominal active power
Q_{max}	[kVAr]	12	Nominal reactive power
R_l	[Ω]	2.4207	Minimum resistive load
L_S	[H]	0.0065	Filter inductance
R_S	[Ω]	0.1	Filter resistor
Z_1	[Ω]	0.1932+ j0.0019	The first inverter line impedance
Z_2	[Ω]	0.3864+ j0.0038	The second inverter line impedance
Z_v	[Ω]	0+ j0.0526	Virtual impedance

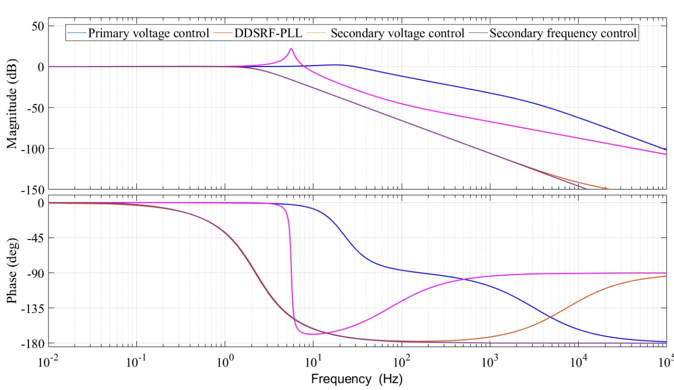

Figure 3. Bode diagram of the system with PI controller in primary and secondary controllers.

TABLE II. Control System Information

Parameter		Value	Description
Primary Control			
f_c	[Hz]	10	Power control cutoff frequency
T_s	[s]	6.4472e-04	DDSRF-PLL setting time
K	-	0.7897	Voltage control Proportional term
T_i	[s]	0.0072	Voltage control Integral term
m_p	-	4.1888e-05	Frequency droop coefficients
n_q	-	5.6474e-04	Amplitude droop coefficients
$\Delta\omega$	[Hz]	0.2	Maximum allowed frequency deviation
ΔV	[V]	0.04	Maximum allowed voltage deviation
Secondary Control			
f_{cpll}	[Hz]	35	DDSRF-PLL cutoff frequency
T_{spll}	[s]	0.01	DDSRF-PLL setting time
K_{pll}	-	2.7181	DDSRF-PLL proportional term
T_{ipll}	[s]	1.2518e+03	DDSRF-PLL integral term
T_{dsc}	[s]	0.05	Secondary control delay time
T_{svsc}	[s]	0.4604	Amplitude secondary control setting time
K_{vsc}	-	2.1719e-04	Amplitude secondary control proportional term
T_{ivsc}	[s]	2.1710e-05	Amplitude secondary control integral term
T_{sfsc}	[s]	0.4705	Frequency secondary control setting time
K_{fsc}	-	9.9955	Frequency secondary control proportional term
T_{ifsc}	[s]	2.4548	Frequency secondary control integral term

TABLE III. PI System Margin Information

LTI System	Gain Margin (dB)	Phase Margin (deg)
Primary voltage control	51.8	112
DDSRF-PLL	83.4	12.3
Amplitude secondary control	89.7	180
Frequency secondary control	71.9	132

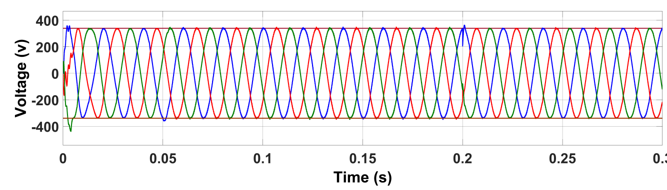

(a)

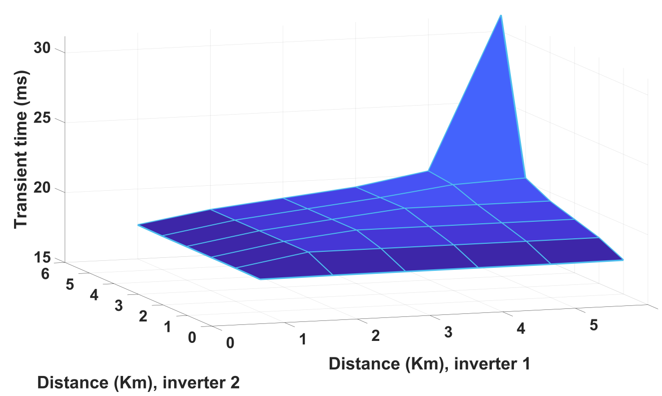

(b)

Figure 4. Output voltage: (a) three phase output voltage, (b) voltage amplitude transient time.

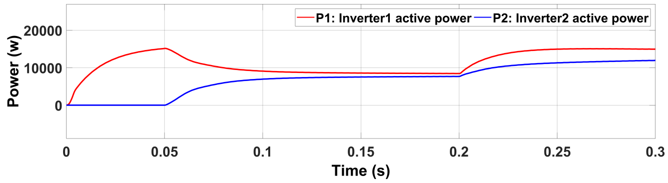

(a)

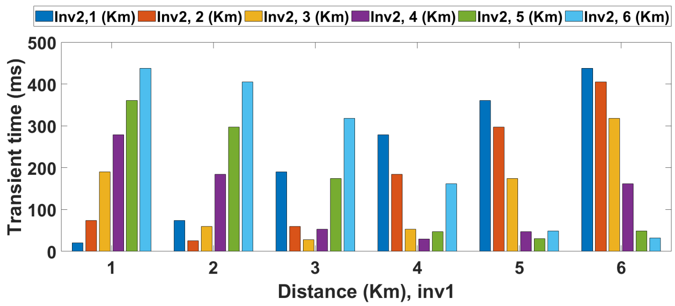

(b)

Figure 5. Output active power sharing among paralleled DGs: (a) Inverters distance from the load: [2,4] (km) , (c) power sharing transient time relation with the distance.

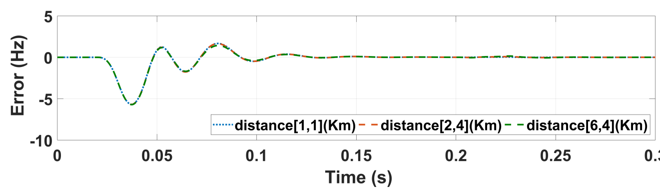

Figure 6. Frequency error from nominal frequency.

varying line impedance. We can conclude that DGs distances, which change the line impedance directly affect the voltage and power-sharing transient time, but not in their steady state.

VI. Conclusion

A step-by-step design of the primary and secondary control systems for the load voltage and frequency of the three-phase paralleled connected VSI-based AC MG is derived. The effect of the DGs remoteness to the load is also considered. The primary and secondary control loops are based on the droop control and autonomous frequency control system. The simulation results show that shifting the DGs distance has a direct influence on the transient time of the voltage and power-sharing. It is important to mention that the main effect for the transient time in power sharing is the difference between inverters' distance and not the distance itself. Also, varying the line impedance has slight effects on the frequency of the system.

References

[1] J. C. Vasquez, J. M. Guerrero, J. Miret, M. Castilla, and L. G. De Vicuna, "Hierarchical control of intelligent microgrids," *IEEE Industrial Electronics Magazine*, vol. 4, no. 4, pp. 23–29, 2010.

[2] B. Lasseter, "Microgrids [distributed power generation]," in *Power Engineering Society Winter Meeting, 2001. IEEE*, vol. 1. IEEE, 2001, pp. 146–149.

[3] C. Moreira, A. G. Madureira, and J. P. Lopes, "Defining control strategies for microgrids islanded operation," 2006.

[4] M. C. Chandorkar, D. M. Divan, and R. Adapa, "Control of parallel connected inverters in standalone ac supply systems," *IEEE Transactions on Industry Applications*, vol. 29, no. 1, pp. 136–143, 1993.

[5] I. S. C. Committee *et al.*, "Ieee standard for interconnecting distributed resources with electric power systems," *IEEE Std1547-2003*, 2009.

[6] Y. Han, H. Li, P. Shen, E. A. A. Coelho, and J. M. Guerrero, "Review of active and reactive power sharing strategies in hierarchical controlled microgrids," *IEEE Transactions on Power Electronics*, vol. 32, no. 3, pp. 2427–2451, 2017.

[7] J. M. Guerrero, M. Chandorkar, T.-L. Lee, and P. C. Loh, "Advanced control architectures for intelligent microgrids-part i: Decentralized and hierarchical control," *IEEE Transactions on Industrial Electronics*, vol. 60, no. 4, pp. 1254–1262, 2013.

[8] K. De Brabandere, B. Bolsens, J. Van den Keybus, A. Woyte, J. Driesen, and R. Belmans, "A voltage and frequency droop control method for parallel inverters," *IEEE Transactions on power electronics*, vol. 22, no. 4, pp. 1107–1115, 2007.

[9] J. C. Vasquez, J. M. Guerrero, M. Savaghebi, J. Eloy-Garcia, and R. Teodorescu, "Modeling, analysis, and design of stationary-reference-frame droop-controlled parallel three-phase voltage source inverters," *IEEE Transactions on Industrial Electronics*, vol. 60, no. 4, pp. 1271–1280, 2013.

[10] J. M. Guerrero, J. C. Vasquez, J. Matas, M. Castilla, and L. G. de Vicuna, "Control strategy for flexible microgrid based on parallel line-interactive ups systems," *IEEE Transactions on industrial Electronics*, vol. 56, no. 3, pp. 726–736, 2009.

[11] M. Ashabani, A.-R. M. Yasser, M. Mirsalim, and M. Aghashabani, "Multivariable droop control of synchronous current converters in weak grids/microgrids with decoupled dq-axes currents," *IEEE Transactions on Smart Grid*, vol. 6, no. 4, pp. 1610–1620, 2015.

[12] N. Rezaei and M. Kalantar, "Smart microgrid hierarchical frequency control ancillary service provision based on virtual inertia concept: An integrated demand response and droop controlled distributed generation framework," *Energy Conversion and Management*, vol. 92, pp. 287–301, 2015.

[13] J. M. Guerrero, J. C. Vasquez, J. Matas, L. G. De Vicuña, and M. Castilla, "Hierarchical control of droop-controlled ac and dc microgrids—a general approach toward standardization," *IEEE Transactions on industrial electronics*, vol. 58, no. 1, pp. 158–172, 2011.

[14] A. Madureira, C. Moreira, and J. P. Lopes, "Secondary load-frequency control for microgrids in islanded operation," in *Proc. Int. Conf. Renewable Energy Power Quality*, 2005.

[15] Q. Shafiee, J. M. Guerrero, and J. C. Vasquez, "Distributed secondary control for islanded microgrids—a novel approach," *IEEE Transactions on power electronics*, vol. 29, no. 2, pp. 1018–1031, 2014.

[16] A. Mehrizi-Sani and R. Iravani, "Potential-function based control of a microgrid in islanded and grid-connected modes," *IEEE Transactions on Power Systems*, vol. 25, no. 4, pp. 1883–1891, 2010.

[17] J. M. Guerrero, N. Berbel, L. G. de Vicuña, J. Matas, J. Miret, and M. Castilla, "Droop control method for the parallel operation of online uninterruptible power systems using resistive output impedance," in *Applied Power Electronics Conference and Exposition, 2006. APEC'06. Twenty-First Annual IEEE*. IEEE, 2006, pp. 7–pp.

[18] E. Planas, A. Gil-de Muro, J. Andreu, I. Kortabarria, and I. M. de Alegría, "General aspects, hierarchical controls and droop methods in microgrids: A review," *Renewable and Sustainable Energy Reviews*, vol. 17, pp. 147–159, 2013.

[19] U. B. Tayab, M. A. B. Roslan, L. J. Hwai, and M. Kashif, "A review of droop control techniques for microgrid," *Renewable and Sustainable Energy Reviews*, vol. 76, pp. 717–727, 2017.

[20] P. Rodríguez, J. Pou, J. Bergas, J. I. Candela, R. P. Burgos, and D. Boroyevich, "Decoupled double synchronous reference frame pll for power converters control," *IEEE Transactions on Power Electronics*, vol. 22, no. 2, pp. 584–592, 2007.